

BL14B1

QST Quantum Dynamics II

1. Introduction

BL14B1 is designed for various types of diffraction experiment and X-ray absorption fine structure (XAFS)-type spectroscopy measurements in the energy ranges of 5–90 keV for monochromatized beams and 5–150 keV for white beams. The main optics refers to the standard SPring-8 bending-magnet system with two mirrors and a fixed-exit double-crystal monochromator. These optical elements can be removed completely for an experiment involving white X-rays. This beamline has two experimental hutches. One is a white X-ray hutch dedicated to high-pressure and dispersive XAFS experiments with white X-rays. The other is a monochromatic X-ray hutch dedicated to XAFS, X-ray diffraction measurements, and X-ray irradiation experiments. BL14B1 can be a one-stop platform for developments of novel functional materials by the complementary use of white and monochromatized X-rays.

A κ -type multi-axis diffractometer installed

in the monochromatic X-ray hutch was moved to another beamline. Another four-circle X-ray diffractometer has been installed in the hutch. A system for X-ray irradiation experiments on tumors is introduced (Fig. 1) on the diffractometer. The irradiated X-ray beam position can be monitored in two ways using the system. One is using a coaxial laser irradiation system. The coaxial green laser irradiates the position where X-rays irradiate. The laser position is monitored using a digital optical microscope. The other is using a beam monitor with a CMOS camera, which enables us to monitor the irradiation position directly by observing transmission images.

2. High-pressure and high-temperature experiments

High-pressure and high-temperature syntheses have been performed at the white X-ray hutch. *In situ* synchrotron radiation X-ray diffraction measurements can detect structural changes of a

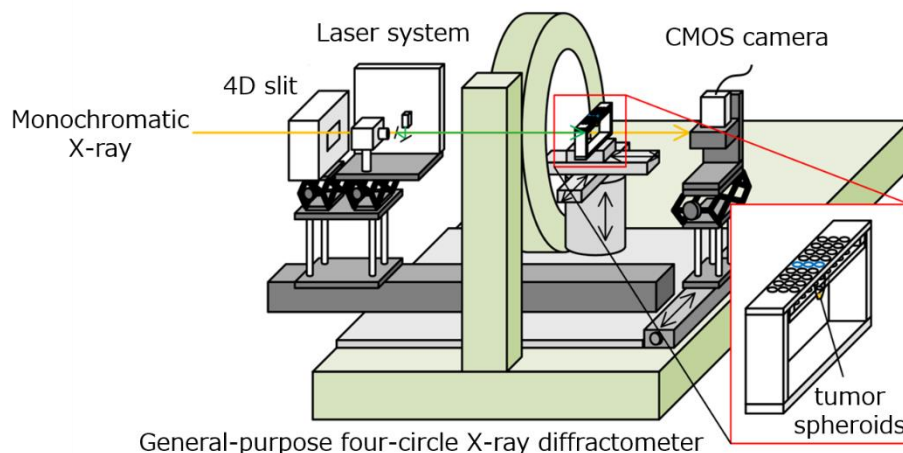


Fig. 1. Schematic of a newly introduced system for X-ray irradiation experiments on tumors.

sample under high pressure and temperature. Consequently, the synthetic conditions of novel materials can be easily searched. Additionally, the system can investigate the reaction mechanisms.

Currently, research focuses on synthesizing novel hydrides. In FY2020, a novel Co-Ti alloy hydride was investigated [1]. Figure 2 shows a series of X-ray diffraction profiles of Co_3Ti alloy in fluid hydrogen at 9 GPa. The discontinuous lattice expansion was observed at 900°C, indicating that $\text{Co}_3\text{TiH}_{-4}$ with a Cu_3Au -type structure was formed. The formed hydrides evolved hydrogen partially, and $\text{Co}_3\text{TiH}_{-1}$ was recovered at ambient conditions. The partial evolution of hydrogen can be explained by the difference in hydrogen stability at different hydrogen sites. In Co_3Ti alloy, there are two

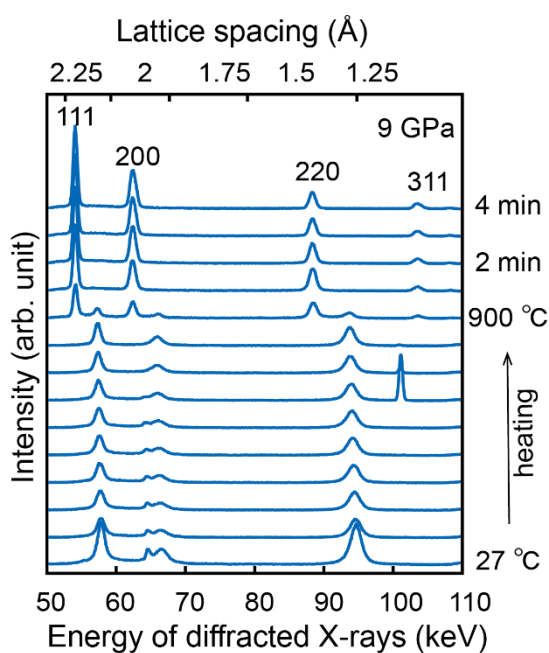


Fig. 2. Series of X-ray diffraction profiles of Co_3Ti alloy in fluid hydrogen at 9 GPa. The discontinuous lattice expansion was observed at 900°C, which was caused by the formation of $\text{Co}_3\text{TiH}_{-4}$ with a Cu_3Au -type structure.

hydrogen sites: an octahedral site consisting of six cobalt atoms and that consisting of four cobalt and two titanium atoms. Hydrogen atoms in the latter site are less stable and evolved during decompression, whereas hydrogen atoms in the former site are more stable and were recovered at ambient conditions.

3. Stress

The strain scanning measurements using the energy-dispersive X-ray diffraction method were performed using high-energy white X-rays with a Ge solid-state detector. By this measurement technique, the effects of residual stress on the hydrogen embrittlement behavior of a tempered martensitic steel sheet with 1-GPa-class tensile strength stretch-formed by a hemisphere punch were investigated. In addition, stress and plastic strain distributions in the specimen were analyzed by the finite element method (FEM). These analyses showed that the high tensile stress in the circumferential direction was in the foot of the impression, corresponding to the direction of the crack growth. FEM analysis revealed that the high triaxial stress was located in the foot, suggesting hydrogen accumulation [2]. The effects of residual stress and plastic strain on the hydrogen embrittlement of a stretch-formed, transformation-induced, and plasticity-aided martensitic steel sheet were also investigated using the same system [3].

We have been developing a double-exposure method (DEM) with high-energy white X-rays for the internal stress/strain evaluation of metals with quasi-coarse grains. In FY2020, we investigated the effects of the measured Q-space range and camera length on the accuracy of the measured strain. It was confirmed that an expansion of the measured Q-

space range had no effect on the improvement of the accuracy of the measured strain and that increasing the distance between a sample and a detector was effective for improving the accuracy. In addition, the accuracy is suggested to be high by calculating it using Laue spots that do not contain extra intensities caused by higher-order X-rays.

4. XAFS

XAFS measurements using an energy-dispersive optical system were performed in the white X-ray hutch as well as a conventional optical system in the monochromatic X-ray hutch [4-7]. Various XAFS measurements from high-speed chemical reactions to low-concentration additives can be performed.

Several *in situ* observation conditions can be prepared in the energy-dispersive optics hutch. Remote control systems such as gas flow controllers, switching valves, potentiostats, and injectors are always available. Some experiments using laser systems are also operated. Time-resolved measurements are performed for gas conversion reactions, electrode reactions, ligand substitution reactions, and so forth. In FY2020, the hydrogenation and dehydrogenation reactions of some precious metal nanoparticles were observed by time-resolved XAFS measurement at a rate of about 50 Hz, and the reaction mechanisms of hydrogen molecules and atoms were clarified.

In the conventional optics system, measurements of low-concentration XAFS are performed using a 36-element solid-state detector. For example, local structure measurements of Cs-biotite at Cs K-edge XAFS were carried out from the viewpoints of stable storage and volume reduction of radioactive wastes. A correlation between the layered structure and the Cs sorption

site was detected by the observation of the size-controlled samples. We are continuing research to determine the relationship between the clay structure and the sorption state of cesium ions, thereby leading to the mobility evaluation and selective collection of radioactive cesium ions.

5. X-ray irradiation effects on a tumor

The X-ray irradiation effects on a tumor were investigated for Auger therapy. Tumor spheroids containing I-loaded nanoparticles were irradiated with synchrotron radiation monochromatic X-rays [8]. The destruction of tumor spheroids was observed in the same manner as that of tumor spheroids containing Gd-loaded nanoparticles, which was reported in FY2019. DNA double-strand breaks were also detected after the X-ray irradiation on the tumor spheroids containing I-loaded nanoparticles. The destruction mechanisms of tumor spheroids containing nanoparticles are being investigated.

Hiroyuki Saitoh^{*1}, Ayumi Shiro^{*1}, Takahisa Shobu^{*2}, and Daiju Matsumura^{*3}

^{*1} High Pressure Science and Stress Research Group, Synchrotron Radiation Research Center, Kansai Photon Science Institute, Quantum Beam Science Research Directorate, National Institutes for Quantum and Radiological Science and Technology

^{*2} Analytical Sciences Development Research Group, Materials Sciences Research Center, Japan Atomic Energy Agency

^{*3} Environment and Materials Dynamics Research Group, Materials Sciences Research Center, Japan Atomic Energy Agency

References:

- [1] Saitoh, H. et al. (2020). *Int. J. Hydrogen Energy* **45**, 33675.
- [2] Shibayama, Y. et al. (2021). *ISIJ Int.* **61**, 1322.
- [3] Hojo, T. et al. (2020). *Corros. Sci.* **177**, 108957.
- [4] Lai, W. et al. (2020). *Angew. Chem. Int. Ed.* **59**, 22171.
- [5] Saeki, M. et al. (2020). *Anal. Sci.* **36**, 1371.
- [6] Itoi, H. et al. (2020). *J. Phys. Chem. C* **124**, 15205.
- [7] Song, C. et al. (2020). *RSC Adv.* **10**, 19751.
- [8] Higashi, Y. et al. (2021) *Sci. Rep.* **11**, 14192.